Transition from zero-dimensional superparamagnetism to two-dimensional ferromagnetism of Co clusters on Au(111)

S. Padovani, I. Chado, F. Scheurer, and J. P. Bucher*
Institut de Physique et Chimie des Matériaux de Strasbourg, UMR 7504 CNRS–Université Louis Pasteur, 23 rue du Loess, F-67037 Strasbourg Cedex, France
(Received 9 November 1998)

The early growth stages of Co structures on Au(111) have been analyzed by scanning tunneling microscopy and their magnetic properties simultaneously measured, *in situ*, by Kerr effect and, *ex situ* by superconducting quantum interference device. With increasing cobalt coverage, cobalt clusters, organized on the lattice of the $22\times\sqrt{3}$ zigzag reconstruction coalesce into one-dimensional (1D) chains at a coverage of 1.0 monolayer (ML) and then into a nearly continuous film at 2 ML. While this well-defined growth mode is dictated by the presence of ordered point dislocations at the zigzag reconstruction of the relaxed gold surface, anomalous nucleation and growth is also observed when large domains of strained linear reconstructions are present. Two families of clusters must then be considered with important consequences for magnetic properties. When only the zigzag reconstruction is present, the onset of long-range, 2D ferromagnetism is observed at a coverage of 1.6 ML of cobalt. A Monte Carlo simulation of an anisotropic Heisenberg model describes well transitions from 0D cluster superparamagnetism, to 1D Ising behavior and finally to 2D ferromagnetism as a function of cobalt coverage, in good agreement with experimental results. [S0163-1829(99)04617-2]

I. INTRODUCTION

Although numerous studies were devoted to the growth and magnetic properties of Co structures on various types of Au substrates (see, for example, Refs. 1–14), up to now a precise *in situ* correlation of the Co cluster morphology and the magnetic behavior in the early growth stages is still missing. In particular, the onset of ferromagnetism has not been analyzed in detail. Ferromagnetism with perpendicular anisotropy is generally observed above 2 monolayers (ML) Co coverage. Below 1 ML, a superparamagnetic phase has been attributed to the presence of small Co clusters.[13,14] What is happening between 1 and 2 ML is still subject to debate. Most of the magnetic studies were performed *ex situ* on gold-capped Co layers and multilayer samples without any morphology analysis. Whenever correlations between topography and magnetism have been achieved, interesting dimensional effects have been observed as in the case of Fe deposited on a vicinal Cu(111) (Ref. 15) and W(110) surfaces.[16] An attempt to characterize both morphology and magnetic properties has been made recently on a wedge-shaped Co/Au/mica sample[13] but unfortunately the sample could be characterized magnetically only *ex situ*.

In this paper, the first growth stages of Co on Au(111) have been followed by scanning tunneling microscopy (STM) and the magnetic properties analyzed simultaneously by means of *in situ* Kerr effect. Growth is shown to depend strongly on the shape of the underlying reconstructions. In addition to the well-known ordered cobalt clusters that grow on the zigzag reconstructions,[1] we observe randomly ramified islands which we attribute to growth on linear reconstructions. Strain induced linear reconstructions appear when defects, such as screw dislocations, are present on the surface. We therefore conclude that the particular magnetic properties of Co/Au(111) strongly depend on the proportion of zigzag and linear domains. On a well-prepared gold single crystal, chain-like structures form at about 1.0 ML Co coverage as a result of cluster coalescence along the rows. Upon increasing the coverage, the free space between chains is filled by new clusters, nucleating and growing between adjacent chains, until a nearly continuous, granular, 2-ML-thick film is formed. A long-range two-dimensional (2D) ferromagnetic order first appears at 1.6 ML. The onset of the ferromagnetic order can be understood in terms of a transition from a 1D system without long-range correlations to a percolating long-range 2D magnetic order as supported by Monte Carlo simulations.

II. EXPERIMENT

The experiments were carried out in an ultrahigh vacuum chamber which consists of a home-built STM and a four-grid diffraction optics also used as a retarding field analyzer for chemical analysis. A movable electromagnet and four viewports allow us to measure *in situ* the magneto-optical Kerr effect in the longitudinal and polar geometries. A maximum field of 650 Oe is reached. The sample temperature can be varied between 30 and 1500 K. Cobalt is evaporated from a high-purity rod, and gold from a boron nitride crucible, heated by electron bombardment. Both evaporation cells are equipped with flux monitors calibrated by STM.

Two types of samples were used: (i) a gold single crystal and (ii) an Au(111) film grown on mica. The Au/mica substrates consist of (111) textured grains randomly disoriented. The gold layers are grown in a separate chamber and are about 100 nm thick. The single-crystal and the gold film on mica are prepared in the same way by Ar^+ ion sputtering at 1 kV and annealing cycles (maximum annealing temperature: 1000 K). This procedure leads to large flat terraces presenting the $22\times\sqrt{3}$ zigzag reconstruction. Each sample is analyzed by STM, polar, and longitudinal Kerr effect. After the *in situ* characterization, the Co/Au/mica samples are encased with about 50 ML gold and further analyzed *ex situ* by superconducting quantum interference device (SQUID) magnetometry.

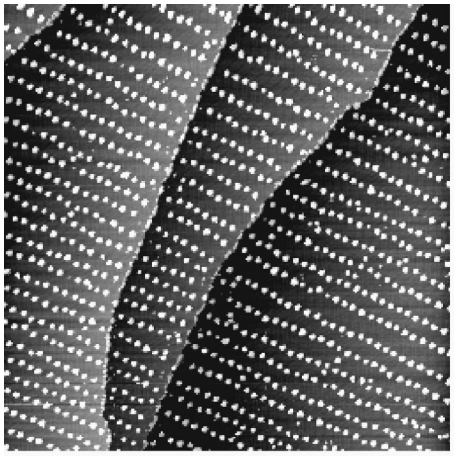

FIG. 1. 0.3 ML Co grown at room temperature on a Au(111) single crystal. 300×300 nm^2.

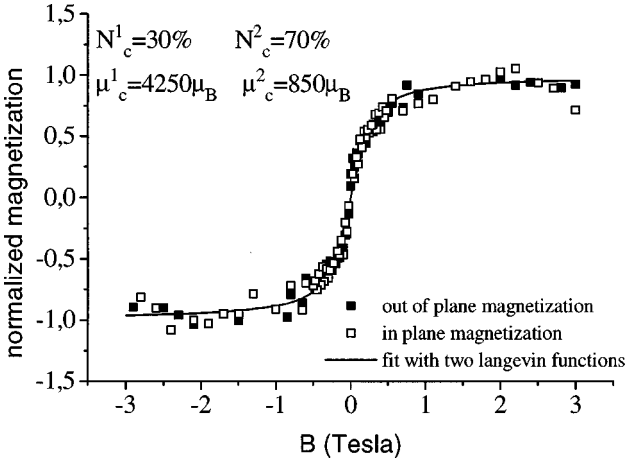

FIG. 2. SQUID magnetization curves recorded at 290 K for 0.4 ML Co on Au(111)/mica. For giant magnetic moments μ_c^1 and μ_c^2 estimated from STM pictures, the fit with a sum of two Langevin functions give the proportion of each of the two populations N_c^1 and N_c^2.

III. RESULTS AND DISCUSSION

Scanning tunneling microscopy of room-temperature-grown Co structures on Au(111) show that Co atoms build small bilayer-high clusters in the early growth stage.[1] Figure 1 shows a STM picture obtained for 0.3 ML Co deposited on a gold single crystal (since the Co clusters are bilayer-high, this means that only 15% of the gold surface is covered). At this coverage, no Kerr signal is obtained *in situ* for a temperature between 30 and 450 K, neither in the polar nor in the longitudinal geometry. Gold-covered Co/Au/mica samples at this coverage have been shown to behave superparamagnetically with a saturation field above 10 kOe.[13] At 650 Oe (the maximum field in our setup) the signal is too weak to be measured. Therefore a Co film of comparable thickness has been prepared on a Au/mica sample, analyzed by STM and Kerr (we checked, furthermore, that no *in situ* Kerr signal was observable), then covered with about 50 ML gold and measured *ex situ* by SQUID. Gold encasing does not alter the cobalt cluster morphology as demonstrated by an STM study.[17] Figure 2 shows the SQUID magnetization curves obtained at room temperature for in-plane and out-of-plane applied fields. Both curves are identical with zero remanent magnetization, clearly indicating a superparamagnetic behavior[18] above the blocking temperature. The possible increase of the perpendicular anisotropy barrier due to the new interface, created by the gold overlayer, is not sufficient to block the cluster's magnetization at room temperature.

Results from the literature[13,14] agree that superparamagnetism is observed below 1 ML Co coverage. Above this value, the results disagree somewhat, regarding the thickness limit for which a hysteretic magnetization curve is obtained. There are also large discrepancies in the average cluster size estimated from the Langevin function.[13,14] For a 0.4 ML Co coverage on the Au(111)/mica sample, the fit with a single Langevin function of the magnetization curves in Fig. 2 gives a cluster size of 2500 atoms, approximately (assuming a magnetic moment per Co atom of $1.7\mu_B$), whereas the organized clusters contain only about 500 atoms, as estimated from STM images. In order to explain the difference, one has to examine more carefully the growth process of Co on Au(111)/mica samples.

While, on a well-prepared gold single crystal, one can consider that organized dots (like those in Fig. 1) are representative of the whole surface, this is no longer true for Co/Au/mica samples. This remark is particularly relevant to magnetic measurements, since SQUID averages the magnetic properties of the clusters over the whole sample. Figure 3 shows a STM picture of the sample used for the *ex situ* SQUID measurement, prior to gold encasing. Three types of Co clusters can be identified: (i) Co clusters nucleated in the step edges, (ii) Co clusters building a regular array, and (iii) randomly distributed Co clusters. The type (iii) clusters contain at least four times more atoms than the clusters in region (ii). The origin of the different growth modes is directly related to the particular reconstruction of the gold surface.

The clean surface of a well-prepared Au(111) single crystal shows large atomic flat terraces (as large as 300×300 nm) presenting the zigzag $22\times\sqrt{3}$ reconstruction (the so-called herringbone reconstruction).[19–21] It consists of an alternation

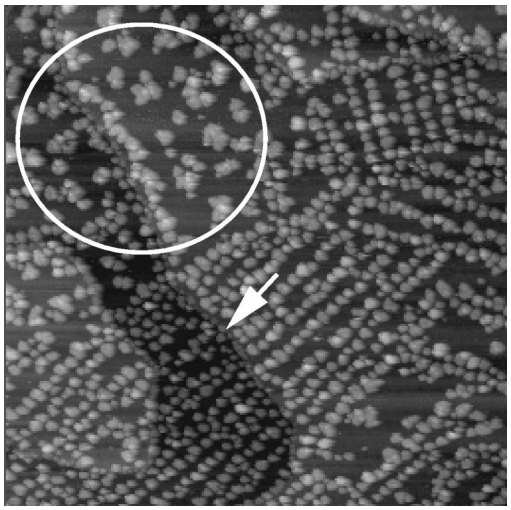

FIG. 3. 0.4 ML Co deposited at 300 K on Au(111)/mica. 250×250 nm^2 region showing three types of clusters: (1) On regular arrays, (2) randomly nucleated (circled region), and (3) nucleated in step edges (indicated by an arrow).

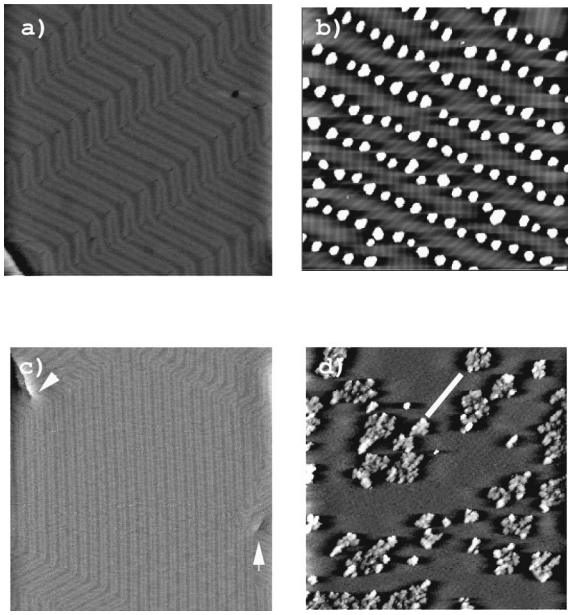

FIG. 4. (a) Zigzag reconstruction on a gold single-crystal. 100 $\times$100 nm^2; (b) 0.3 ML Co deposited at 300 K on single gold crystal. 100$\times$100 nm^2; (c) linear reconstruction on Au/mica. Arrows indicate the positions of screw dislocations. 150$\times$150 nm^2; (d) random-shaped islands on linear reconstruction for 0.6 ML Co. The white arrow indicates the direction of the linear reconstruction. 245 $\times$245 nm^2.

of fcc and hcp stacking domains on gold surface [Fig. 4(a)]. The domains are separated by soliton walls corresponding to atoms on bridge sites (bright lines on STM picture). The widths of the fcc and hcp domains are 42 and 22 Å, respectively. The zigzag domain shape allows to further release surface stress.[22] Room-temperature-deposited Co atoms nucleate preferentially at the point dislocations of the zigzags. At low coverage, a regular array of small disconnected bilayer high Co clusters form spontaneously [Fig. 4(b)]. When defects like coin dislocations and screw dislocations appear on the gold surface they perturb the zigzag reconstruction and stabilize the linear reconstruction [see arrows in Fig. 4(c)]. This linear reconstruction, running along a $\langle 112 \rangle$-type direction,[23] does not have point dislocations which could act as preferential nucleation sites and the Co clusters grow thus randomly [Fig. 4(d)]. The linear reconstruction, and hence the third type of Co clusters, are not observed on the single crystal since the density of defects is very low compared to the Au/mica substrate. The fact that the random-shape islands of Fig. 4(d) are elongated in the direction of the reconstruction accounts for anisotropic diffusion. It is worth noting that the weak corrugation of the reconstruction (less than 0.2 Å) is sufficient to induce this preferential diffusion.

In order to estimate the proportion of clusters from type (ii) and (iii), the magnetization curve (Fig. 2) is fitted by a sum of two Langevin functions L, corresponding to clusters of $N_1 = 500 \pm 100$ and $N_2 = 2500 \pm 500$ Co atoms, respectively. The contribution of the clusters in the step edges is supposed to be negligible because of their small proportion and size. The normalized magnetization is given by

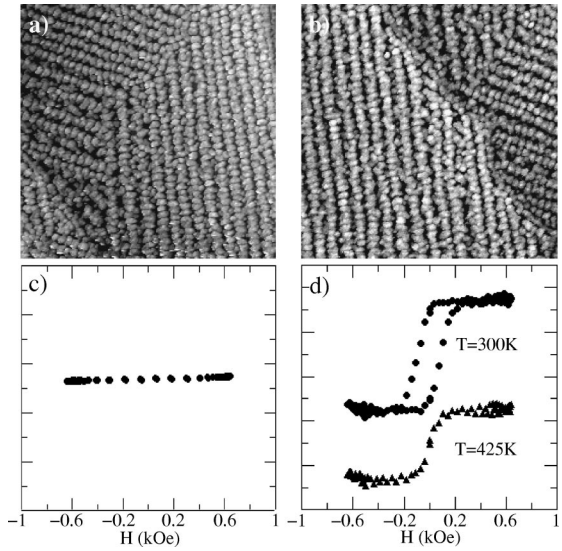

FIG. 5. (a) 1.4 ML Co deposited at 300 K on a Au(111) single crystal, 200$\times$200 nm^2; (b) 1.6 ML Co deposited at 300 K on a Au(111) single crystal, 200$\times$200 nm^2; (c) *in situ* polar Kerr signal of (a) recorded at 300 K; (d) *in situ* polar Kerr signal of (b) recorded at 300 K (circle) and at 425 K (triangle).

$$M/Ms = \frac{N_1^c \mu_1^c}{N_1^c \mu_1^c + N_2^c \mu_2^c} L(\mu_1^c H/k_B T) + \frac{N_2^c \mu_2^c}{N_1^c \mu_1^c + N_2^c \mu_2^c} L(\mu_2^c H/k_B T), \quad (1)$$

where N_1^c and N_2^c are the numbers of the small and big clusters, $\mu_1^c = N_1 \mu_{\mathrm{Co}}$ and $\mu_2^c = N_2 \mu_{\mathrm{Co}}$ their giant magnetic moments ($\mu_{\mathrm{Co}} = 1.7 \mu_B$). The fit gives a proportion of 30 ± 10 % big [type (iii)] and 70 ± 10 % small [type (ii)] clusters, consistent with the STM data. Although the big clusters are a minority, they contribute the major part of the magnetic signal.

The anomalous growth of Co observed on the Au/mica sample explains not only the difficulty to obtain reliable cluster sizes by fitting the magnetization curves with a Langevin function, but also the discrepancies in the critical thickness (1.2–2.0 ML), found in the literature for the ferromagnetic transition.[13,14] Indeed, a broad distribution of cluster sizes will smear out the distribution of blocking temperatures and prevent the measure of a well-defined critical thickness.

In contrast, let us now analyze the well-defined growth on a gold single crystal. Assuming a hexagonal shape of the clusters (see Fig. 6), a separation of 75 Å between clusters along a row and a distance between rows of 130 Å, the clusters within a row should coalesce at a coverage approaching 1.0 ML. Although a detailed STM analysis shows that at a coverage of 1.4 ML the clusters may still be separated by small gaps [see Fig. 5(a)], the gaps are so small that it is reasonable to assume that the clusters are coupled magnetically along rows above 1 ML. Above this limit, additional clusters also start nucleating between adjacent chains.

Although no obvious topographic differences are observed when increasing slightly the coverage from 1.4 ML [Fig. 5(a)] to 1.6 ML [Fig. 5(b)], the polar Kerr signal shows

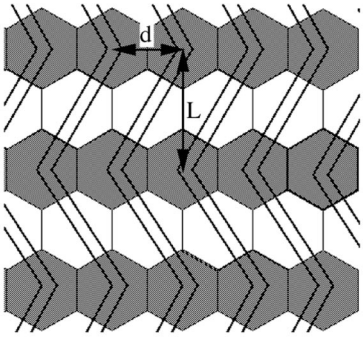

FIG. 6. Schematic representation of the clusters (gray hexagons) nucleated on the zigzag reconstruction. The distance between adjacent clusters is $d=75$ Å and between rows $L=d\sqrt{3}\approx 130$ Å.

a dramatic change: at 1.4 ML [Fig. 5(c)], no Kerr signal is observed in an applied field of 650 Oe, whereas at 1.6 ML [Fig. 5(d)], a hysteresis loop with 100% remanence is obtained. The very abrupt transition suggests a magnetic percolation mechanism from 1D chains towards a 2D long-range ferromagnetic order with perpendicular anisotropy.

In the following, we analyze the evolution of the magnetic state of the Co structures on Au(111) as a function of Co coverage. The system is appropriately described by an anisotropic 2D Heisenberg model of giant magnetic moments associated with each cluster. The clusters are assumed to be arranged on an $N\times N$ hexagonal lattice (see Fig. 6). The increasing cobalt coverage is described by introducing an occupation matrix defined by $\varepsilon_i=1,0$ depending if the site $i=(x_i,y_i)$ is occupied by a cluster or not. The relation between the Co coverage Θ and ε_i is given by $\Theta=(2/N^2)\Sigma_i\varepsilon_i$, the factor 2 accounts for the fact that clusters are bilayers. The system is described by the following Hamiltonian:

$$H=-\frac{\gamma S}{2}\sum_{i,j}\ \delta_{i,j}\boldsymbol{\sigma}_i\varepsilon_i\cdot\boldsymbol{\sigma}_j\varepsilon_j-K_uV_0\sum_i\ (\sigma_i^z\epsilon_i)^2$$

$$-M_0B\sum_i\ \sigma_i^z\varepsilon_i, \qquad (2)$$

where $\boldsymbol{\sigma}_i$ is the normalized giant moment of the cluster at the site i. The first term $\gamma S\boldsymbol{\sigma}_i\cdot\boldsymbol{\sigma}_j$ accounts for the wall energy $(\gamma S/2)(1-\boldsymbol{\sigma}_i\cdot\boldsymbol{\sigma}_j)\delta_{i,j}$ between first neighbors with $\delta_{i,j}=1$ (0) if i and j are (not) first neighbors, γ the surface energy density, and S the surface of the wall. This term expresses the necessity to create a magnetic wall between adjacent clusters if their giant moments are in opposite direction; it supposes that the wall thickness is negligible. Thus a necessary condition for our model to be relevant is that the width of the magnetic wall w is smaller than the diameter of the clusters; an upper limit estimation of w is given by the micromagnetic theory $w\propto\sqrt{A/K_u}\approx 30$ Å. The second term is the anisotropic energy with K_u the anisotropic constant and V_0 the cluster volume. The last term is the Zeeman coupling where M_0 is the giant moment of the cluster and B the applied perpendicular field. In the limit where the clusters are disconnected ($S=0$, 0D limit), we retrieve the Hamiltonian of a superparamagnetic assembly of clusters.

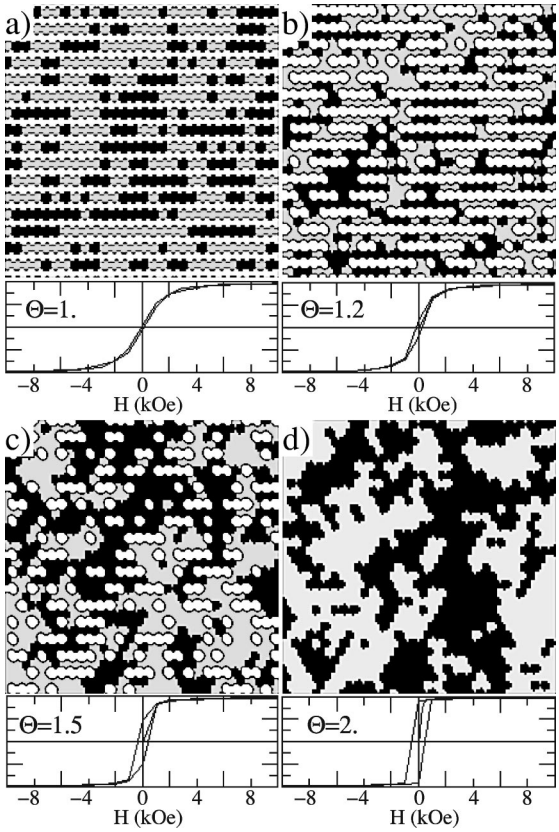

FIG. 7. Demagnetized σ^Z map of 30×30 sites for different coverages Θ. Unoccupied sites are in white, occupied sites with up (down) magnetization are in grey (black). The corresponding first magnetization curves and full hysteresis loops are shown.

An order of magnitude of γ is given by the Bloch-wall energy $\gamma=2\sqrt{AK_u}\approx 10^{-3}$ J/m^2 [$K_u\approx 1$ MJ/m^3,[6] $A\approx 1.10^{-11}$ J/m (Ref. 24) although our consideration does not rely on a particular type of wall. Assuming $S\approx 300$ Å, γS is found of the order of 200 K. However, the micromagnetic theory to evaluate γ is very critical at the Co thicknesses considered here, and the surface contact S between adjacent clusters is difficult to estimate from STM pictures. Therefore we determine γS from the critical temperature (T_c) of the system. The 2D Heisenberg model with uniaxial anisotropy presents a critical temperature which is equal, within a good approximation, to the one of the Ising model, provided that $\gamma S/K_u<0.4$.[25] Since for the hexagonal lattice $T_c\cong 3.62(\gamma S/k_B)$,[26] the value of $\gamma S=125$ K is determined from the critical temperature $T_c=450$ K, previously measured for a 1.6 and 3.2 ML Co coverage.[10] Note that the low experimental saturation field close to T_c [Fig. 5(d)] supports a transition from a ferromagnetic order to a superparamagnetic uncorrelated spin-block behavior rather than to a paramagnetic state as discussed in Ref. 27. Assuming $V_0\approx 20$ nm^3, the anisotropy barrier height K_uV_0 is about 1000 K. Comparing each cluster to a giant dipole $M_0\approx 1000$ K T^{-1}, the dipolar contribution between first neighbors is calculated to be of the order of 1 K, thus negligible.

The domain pattern and the magnetization curves are calculated as a function of the Co coverage by Monte-Carlo

simulations, using a Metropolis algorithm.[28] The calculations are performed on a 256×256 triangular grid with cyclic boundary conditions. We start from a 1 ML coverage corresponding to isolated chains (see Fig. 6) and allow bilayer clusters to nucleate randomly between the chains until the film completion at 2 ML is obtained. The probability of site occupation is $\Theta-1$, since $\Theta=2$ ML when all sites are occupied.

Demagnetized σ^z maps and magnetization curves are shown in Fig. 7 for different coverages at $T=300$ K. Below 1.5 ML [Figs. 7(a) and 7(b)], the thermal disorder destroys the long-range correlation between clusters; there is no, or only weak, remanence and a high saturation field. At 1.5 ML [Fig. 7(c)], the domain size increases strongly and a hysteresis loop appears, with a 60% remanence and a saturation field of 2 kOe (the saturation field is defined at 90% of the saturation on the first magnetization curve). At two monolayers [Fig. 7(d)], large domains of about 1 μm^2 are obtained and a square hysteresis loop with a low saturation field (500 Oe) is obtained. One can notice that between 1 and 2 ML, $\langle\sigma^z\rangle$is about 68 ± 2 % in the demagnetized state (independent of Θ) showing the Ising-like behavior of the system.

From the calculation, it clearly appears that the saturation field steadily decreases as a function of coverage from a value of 4.2 kOe at 1 ML [Fig. 7(a)] to a value of 0.5 kOe at 2 ML [Fig. 7(d)], corresponding to a linear decrease of 400 Oe every tenths of a monolayer. This may explain, why experimentally, a hysteresis abruptly appears when the field excursion is large enough to leave the reversible regime (this occurs at 650 Oe for 1.6 ML at 300 K).

IV. CONCLUSION

The nucleation of Co has been analyzed by STM on a Au(111) single crystal and on Au(111)/mica substrates. On the single crystal, the Co clusters form at low coverage a regular array on the whole sample surface because of the preferential nucleation of Co at the point dislocations of the $22\times\sqrt{3}$ herringbone surface reconstruction. Increasing the coverage leads to growth and coalescence of the clusters into 1D chains, inducing a transition from a superparamagnetism to a 1D magnetism without long-range correlations between clusters. Correlations appear between 1 and 2 ML while islands nucleate between chains. The main effect of the increasing correlation is a strong decrease of the saturation field. At 1.6 ML the saturation field is less than 650 Oe.

On Au/mica samples, a large distribution of Co cluster sizes is observed. Cobalt cluster arrays, similar to those on a single crystal, are observed together with larger randomly nucleated clusters. This is due to the coexistence, on the Au/mica substrate, of the normal herringbone surface reconstruction and of a perturbed linear reconstruction. The large size distribution of the Co clusters on Au/mica substrates may explain the discrepancies of the thickness values for which a ferromagnetic behavior for the Co clusters is observed.

ACKNOWLEDGMENTS

We are very grateful to R. Poinsot for the SQUID measurements. This work was supported by the Centre de la Recherche Scientifique (CNRS-ULTIMATECH Program).

*Author to whom correspondence should be addressed. Electronic address: bucher@morgane.u-strabg.fr

[1] B. Voigtländer, G. Meyer, and N. M. Amer, Phys. Rev. B **44**, 10 354 (1991).
[2] C. Chappert, K. Le Dang, P. Beauvillain, H. Hurdequint, and D. Renard, Phys. Rev. B **34**, 3192 (1986).
[3] J. Ferré, G. Penissard, C. Marlière, D. Renard, P. Beauvillain, and J. P. Renard, Appl. Phys. Lett. **56**, 1588 (1988).
[4] P. Bruno, G. Bayreuther, P. Beauvillain, C. Chappert, G. Lugert, D. Renard, J. P. Renard, and J. Seiden, J. Appl. Phys. **68**, 5759 (1990).
[5] J. Pommier, P. Meyer, G. Penissard, J. Ferré, P. Bruno, and D. Renard, Phys. Rev. Lett. **65**, 2054 (1990).
[6] R. Allenspach, M. Stampanoni, and A. Bischof, Phys. Rev. Lett. **65**, 3344 (1990).
[7] M. Speckmann, H. P. Oepen, and H. Ibach, Phys. Rev. Lett. **75**, 2035 (1995).
[8] H. P. Oepen, M. Speckmann, Y. Millev, and J. Kirschner, Phys. Rev. B **55**, 2752 (1997).
[9] R. Jansen, M. Speckmann, H. P. Oepen, and H. van Kempen, J. Magn. Magn. Mater. **165**, 258 (1997).
[10] S. Padovani, P. Molinas-Mata, F. Scheurer, and J. P. Bucher, Appl. Phys. A: Mater. Sci. Process. **66A**, S1199 (1998); S. Padovani, F. Scheurer, and J. A. Bucher, Europhys. Lett. **45**, 327 (1999).
[11] F. J. A. den Broeder, D. Kuiper, A. P. van de Mosselaer, and W. Hoving, Phys. Rev. Lett. **60**, 2769 (1988).
[12] M. D. Ortega, B. Raquet, K. Postava, C. Armand, R. Mamy, M. Goiran, A. R. Fert, and J. C. Ousset, J. Magn. Magn. Mater. **165**, 487 (1997).
[13] H. Takeshita, Y. Susuki, H. Akinaga, W. Mitzutani, K. Ando, T. Katayama, A. Itoh, and K. Tanaka, J. Magn. Magn. Mater. **165**, 38 (1997).
[14] J. Xu, M. A. Howson, B. J. Hickey, D. Greig, E. Kolb, P. Veillet, and N. Wiser, Phys. Rev. B **55**, 416 (1997).
[15] J. Shen, M. Klaua, P. Ohresser, H. Jenniches, J. Barthel, Ch. V. Mohan, and J. Kirschner, Phys. Rev. B **56**, 11 134 (1997), and references therein.
[16] J. Hauschild, H. J. Elmers, and U. Gradmann, Phys. Rev. B **57**, R677 (1998).
[17] J. Wollschläger and N. M. Amer, Surf. Sci. **277**, 1 (1992).
[18] See, e.g., A. H. Morrish, *The Physical Principals of Magnetism* (Wiley, New York, 1965).
[19] J. V. Barth, H. Brune, G. Ertl, and R. J. Behm, Phys. Rev. B **42**, 9307 (1990).
[20] Y. Okwamoto and K. H. Bennemann, Surf. Sci. **186**, 511 (1987).
[21] Ch. Wöll, S. Chiang, R. J. Wilson, and P. H. Lippel, Phys. Rev. B **39**, 7988 (1989).
[22] N. Shobana and D. Vanderbilt, Phys. Rev. Lett. **69**, 1564 (1989).
[23] M. El-Batanouny, S. Burdick, K. M. Martini, and P. Stancioff, Phys. Rev. Lett. **58**, 2762 (1967).
[24] P. E. Tannewald and R. Weber, Phys. Rev. **121**, 715 (1961).
[25] S. T. Chui, Phys. Rev. B **50**, 12 559 (1994).
[26] C. J. Thompson, in *Mathematical Statistical Mechanics*, edited by C. C. Lin, Applied Mathematics Series (MacMillan, New York, 1972), p. 154.
[27] J. A. C. Bland and B. Heinrich Eds., *Ultrathin Magnetic Structures I* (Springer-Verlag, Berlin, 1994), p. 164.
[28] N. Metropolis, A. W. Rosenbluth, M. N. Rosenbluth, and A. H. Teller, J. Chem. Phys. **21**, 1087 (1953).